Ocean Science
Discussions

1 **A measurement system for vertical seawater profiles close to the**

2 **air/sea interface**

3

4 **Richard P. Sims[1,2], Ute. Schuster[2], Andrew. J. Watson[2], Ming Xi. Yang[1], Frances. E.**

5 **Hopkins[1], John. Stephens[1] and Thomas. G. Bell[1,*]**

6

7 [1]{Plymouth Marine Laboratory, Plymouth, United Kingdom}

8 [2]{University of Exeter, Exeter, United Kingdom}

9 *Correspondence to:* T. Bell (tbe@pml.ac.uk)

10

11 **Abstract**

12 This paper describes a Near Surface Ocean Profiler, which has been designed to precisely

13 measure vertical gradients in the top 10 m of the ocean. Variations in the depth of seawater

14 collection are minimised when using the profiler compared to conventional CTD/rosette

15 deployments. The profiler consists of a remotely operated winch mounted on a tethered yet

16 free floating buoy, which is used to raise and lower a small frame housing sensors and inlet

17 tubing. Seawater at the inlet depth is pumped back to the ship for analysis. The profiler can be

18 used to make continuous vertical profiles or to target a series of discrete depths. The profiler

19 has been successfully deployed during wind speeds up to 10 m s^{-1} and significant wave

20 heights up to 2 m. We demonstrate the potential of the profiler by presenting measured

21 vertical profiles of the trace gases carbon dioxide and dimethylsulfide. Trace gas

22 measurements use an efficient microporous membrane equilibrator to minimise the system

23 response time. The example profiles show vertical gradients in the upper 5 m for temperature,

24 carbon dioxide and dimethylsulfide of 0.15 °C, 4 μatm and 0.4 nM respectively.

25

26 **1 Introduction**

27 Exchange between the ocean and atmosphere is an important process for many gases.

28 Important examples include carbon dioxide (CO_2), for which the oceans account for 25% of

1   the sink for anthropogenic emissions (Le Quéré et al., 2016), and dimethylsulfide (DMS),

2   which has an oceanic source and influences cloud properties with implications for the global

3   energy balance   (Quinn and Bates, 2011). The magnitude and direction of air/sea gas transfer

4   is typically represented by Flux=$K\Delta C$ (Liss and Slater, 1974), where ΔC is the concentration

5   difference across the air-sea interface and K is the gas transfer velocity. Direct flux

6   measurements (Bell et al., 2013; Yang et al., 2013; Miller et al., 2010) are only possible for a

7   small number of gases and are not made routinely.   Most flux estimates use a wind speed-

8   based parameterisation of K (e.g. Wanninkhof, 2014) coupled with measurements of ΔC.

9   CO_2 is the most well-observed trace gas in the surface ocean, with 14.5 million measurements

10   compiled into a global database, the Surface Ocean CO_2 Atlas (SOCAT),

11   http://www.socat.info/ (Bakker et al., 2016). Global trace gas databases also exist for gases

12   such as methane and nitrous oxide https://memento.geomar.de/ (Bange et al., 2009),

13   dimethylsulfide http://saga.pmel.noaa.gov/dms/ (Lana et al., 2011) and halocarbons

14   https://halocat.geomar.de/ (Ziska et al., 2013). Accurate estimation of air/sea flux requires

15   concentration measurements that are representative of the interfacial concentration difference.

16   Surface seawater samples are often collected from the underway seawater intake of research

17   vessels, typically at 5-7 m depth. A source of potential error in air/sea flux calculations arises

18   from the assumption of vertical homogeneity within the mixed layer (Robertson and Watson,

19   1992). If vertical concentration gradients exist in the mixed layer, then underway seawater is

20   not representative of the interfacial layer, which could create a global sampling bias (McNeil

21   and Merlivat, 1996).

22   Vertical gradients in trace gas concentrations have been observed under conditions that are

23   favourable for near surface stratification (Royer et al., 2016). At low wind speeds, high solar

24   irradiance can suppress the depth of shear-induced mixing to create a near surface layer

25   several degrees warmer than the water below (Ward et al., 2004; Fairall et al., 1996). Near

26   surface stratification in the marine environment can also be induced by freshwater inputs such

27   as rain (Turk et al., 2010) and riverine discharge. Changes in surface seawater temperature

28   and salinity alter the solubility of dissolved gases and thus the amount available for air/sea

29   exchange (Woolf et al., 2016). Dissolved gases isolated in the upper few metres of the ocean

30   may additionally be modified by physical process such as air/sea exchange and

31   photochemistry. Marine biota confined within the stratified layer (Durham et al., 2009), may

Ocean Science
Discussions

Open Access

EGU

1   also alter trace gas concentrations. For the purposes of this paper, near surface gradients are

2   defined as physical and/or chemical gradients in the upper 10 m of the ocean.

3   Identifying and quantifying near surface gradients in trace gas concentrations is challenging.

4   Ship motion often inhibits near surface measurements made with the standard oceanographic

5   approach of sampling with Niskin bottles mounted on a CTD rosette. Substantial vertical

6   movement of the rosette limits how close to the surface a sample can be taken. For example, a

7   crane arm 4 m above the sea surface and 11 m from the centreline of a ship that is rolling by

8   ±4 degrees will induce ~1.5 m sample depth variation every few seconds. CTD/Niskin bottle

9   sampling requires that the rosette is kept below the sea surface. Sampling within 2 m of the

10   sea surface is often impossible, even under relatively calm conditions.

11   We present a Near Surface Ocean Profiling buoy (NSOP) designed for measuring near surface

12   profiles. The design principles for NSOP were:

13   (1) Platform diameter less than the wavelength of most open ocean waves, allowing it to ride

14   the swell;

15   (2) Short sampling arm close to the sea surface to reduce vertical movements induced by

16   platform motion;

17   (3) Capable of deployment close to the ship (to retrieve water for trace gas analysis), but away

18   from major turbulence and motion due to the ship itself.

19   Example profiles from a cruise on the European continental shelf (*RRS Discovery*, DY033,

20   July 2015) and in the English Channel on board the *RV Plymouth Quest* (part of the Western

21   Channel Observatory, Smyth et al., 2010, April 2014) are discussed.

22

23   **2   Methods**

24   **2.1   Near Surface Ocean Profiler (NSOP) description**

25   NSOP is a repurposed ocean buoy (1.6 m diameter) with a central lifting eyelet (Fig. 1). The

26   top of the buoy is 0.5 m above the sea surface. Mounted on top of the buoy are a line of sight,

27   remotely operated winch (Warrior Winch, model C8000) and a gel battery (Haze, model

28   HZY-S112-230). The winch feeds Kevlar rope through a block and tackle with a 3:1 ratio to

29   reduce rope pay-out speed to ~0.05 m s^{-1}. The block and tackle is attached to the end of an

1   outstretched arm 0.25 m from the outer edge of the buoy. The winch line is attached to an

2   open frame (0.35 m diameter, 0.8 m height) with the capacity to house multiple sensors.

3   Desired sampling depth is targeted using knowledge of the winch pay-out speed. Rope pay-

4   out is then timed with a stopwatch. This approach only approximately regulates the sampling

5   depth because: (i) winch pay-out varies slightly depending on the amount of rope on the

6   spool; and (ii) variable horizontal current strength affects the vertical versus horizontal

7   position of the sampling frame. To minimise horizontal movement of the sampling frame we

8   attached a 10 kg weight to the base of the frame.

9   The primary sensor on the sampling frame is a small CTD (Valeport miniCTD) set to sample

10   at a high frequency (>1 Hz). Under calm conditions it is possible to sample as close as 0.1 m

11   from the air/sea interface when the miniCTD and tubing are mounted near the top of the

12   frame. Rougher conditions demand that the frame be kept deeper (~0.5 m) as motion can

13   momentarily bring the sensors and tubing out of the water. An emergency tag line was

14   attached to the sampling frame in case the winch line failed. Seawater for trace gas analysis

15   was pumped back to the ship at 3.5 L min^{-1} through a 50 m PVC hose (0.5 in ID). A heavy

16   duty peristaltic pump (Watson Marlow, model 701IB/R), primed with water from the ships

17   underway supply was used to overcome the large hydraulic head (~4 m). The open end of the

18   tubing was located at the same depth as the miniCTD. Water arriving to the ship's laboratory

19   was divided, with ~3.0 L min^{-1} for flow-through analysis (e.g. equilibrator for trace gases) and

20   ~0.5 L min^{-1} for discrete samples (e.g. total alkalinity).

21   We assessed the depth resolution capability of NSOP at a particular depth by looking at

22   pressure variations under calm conditions with a fixed amount of winch rope paid out. In calm

23   to moderate conditions (<2.5 m significant wave height) the amount of vertical movement

24   indicated by the standard deviation (SD) in the depth is ±0.18 m (see Fig. S2 in Supplemental

25   information). During 4 deployments in rough conditions (>2.5 m significant wave height), the

26   depth variability increased as the sampling frame was lowered (at 5 m, SD was ±0.275 m).

27   **2.2   NSOP deployment**

28   On a large research vessel such as the *RRS Discovery*, the deployment and recovery of NSOP

29   requires close coordination between the bridge and 3 personnel on deck. NSOP was always

30   deployed while the ship was on station. Ship orientation during deployments was typically

31   with bow into the wind but also accounted for swell and current direction/speed. NSOP was

1   lifted by the aft crane (Fig. 1). Once NSOP was lowered to the surface it was detached from

2   the crane via a quick release. Two slack lines were looped through eyelets on the free-floating

3   NSOP to maintain its position close to the ship. A third slack line was connected to the top of

4   the buoy and passed through a block on a crane arm to maintain distance (minimum 7 m)

5   between NSOP and the ship. The slack lines successfully inhibited the tendency of NSOP to

6   drift horizontally without disrupting its ability to ride the swell. The instrument frame acted

7   like a sea anchor and minimised rotation of NSOP. A 4 m lifting strop used for recovery was

8   connected to the lifting eyelet and loosely lashed to the aft slack line. During retrieval, the

9   slack lines were hauled in and the crane and jib arms brought towards the ship to bring NSOP

10   alongside. The lifting strop was then parted from the slack line and attached to the crane to lift

11   NSOP back on deck. For photographs of each stage of a NSOP deployment and videos of a

12   deployment and in operation, see supplemental material.

13   Turbulence from the ship's propellers has the potential to mix the water column and destroy

14   any near surface gradients. The ship did not use the aft thrusters whenever conditions were

15   suitable (mild sea state, weak currents and no local hazards). Keeping NSOP away from the

16   ship limited disruption of near surface gradients by the thrusters and reduced the risk of line

17   entanglement in the aft propellers. Our winch did not have a groove bar to feed the rope onto

18   the winch drum, leading to an increased likelihood of snagging during spooling. To minimize

19   snagging, the rope was manually fed onto the winch spool before deployments. Visual

20   monitoring of the NSOP frame, slack lines and winch spool is important during deployment.

21   NSOP has been successfully deployed in 'moderate' sea states up to Beaufort force 5 (~10 m

22   s^{-1} wind speed and wave heights of ~2.0 m). Deployment length typically varied from 1-3

23   hours.

24
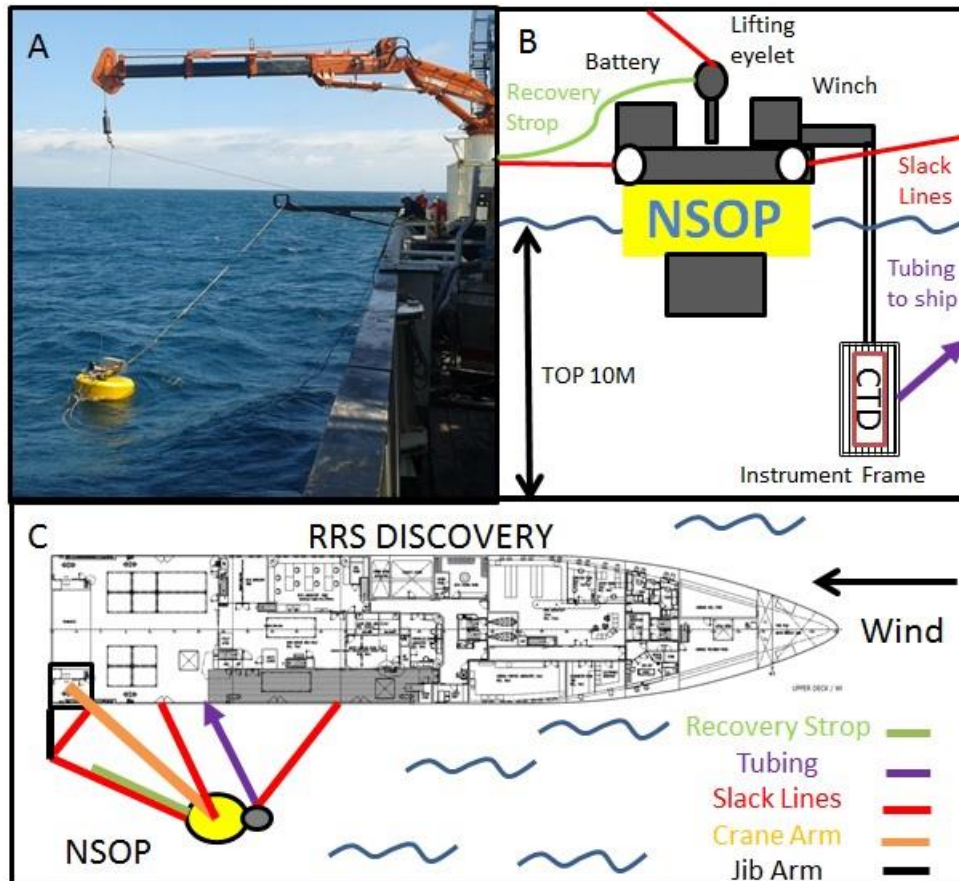
Figure 1: Different points of view of an NSOP deployment: (a) Image from a deployment on *RRS Discovery* in May 2015 (Cruise DY030); (b) Schematic cross section of NSOP including tubing back to ship (purple) and slack lines (red); and (c) Top down schematic from a research ship including ship orientation. Not to scale.

NSOP can be used in two profiling modes: 'continuous' and 'discrete'. Continuous profiling maximises vertical coverage and involves the winch continuously paying rope in and out at ~0.05 m s^{-1}. A complete down/up profile to 10 m can be conducted in approximately 7 min (Fig. 9). Depth resolution during continuous profiling is determined by the measurement response time. Instruments with rapid response times such as the miniCTD temperature and conductivity sensors (0.15 s and 0.09 s) have theoretical depth resolutions of 0.75 cm and 0.45 cm respectively. Actual depth resolution will also be affected by the sampling depth

Ocean Science
Discussions

1   variability of the NSOP instrument frame. A measurement setup with a longer response time

2   (such as for seawater CO_2) requires a different approach (see Section 2.5).

3   During discrete profiling, the winch pays out a fixed amount of rope (typically 0.5 m) and the

4   sampling frame is left at a fixed depth. After a fixed sampling period, more rope is paid out.

5   The process is repeated down and then up such that a set of discrete depths are sampled in a

6   'stepped' profile. The discrete profiling depth resolution is determined by the depth

7   fluctuations when sampling at a fixed depth (see Section 2.1). Discrete profiles are a more

8   appropriate approach for measurement systems with a longer response time. A discrete profile

9   with 0.5 m steps down to 5 m and back to the surface using a 2.5 min sampling period takes

10   about an hour. The sampling period at each depth and frequency/distribution of depths within

11   the profile can be adjusted to suit sampling priorities.

12   The maximum deployment time is limited by the capacity of the winch battery. When under

13   no load, the battery allows for approximately 3 hours of operation in the continuous mode.

14   Discrete profiling requires substantially less winch usage such that battery drainage is even

15   less of a concern.

16   **2.3 CO_2 analysis**

17   The CO_2 measurement system (Fig. 2) is a modified version of the system described by

18   (Hales et al., 2004). Seawater from the NSOP inlet was passed through the equilibrator (see

19   Section 2.3.1) at ~3 L min^{-1} and the flow rate monitored (Cynergy ultrasonic flow meter,

20   model UF25B). A compressed nitrogen gas supply, maintained at a constant flow rate of 100

21   ml min^{-1} (Bronkhurst mass flow controller, model F-201-CV-100) flows through the

22   equilibrator in the opposite direction to the seawater flow. The gas has high water vapour

23   content after equilibration and is dried (Permapure nafion dryer, model MD-110-48S-4). The

24   dried sample then enters the analytical cell of a NDIR Licor 7000, which is protected with a

25   0.2 µm filter (Pall, Acro 50).

26   CO_2 measurements at atmospheric pressure as recommended by Dickson et al. (2007) were

27   not possible due to the nature of the experimental setup. The continuous gas flow through the

28   system caused a small 0.4 kPa pressure increase in the Licor measurement cell. The elevated

29   pressure was taken to be representative of the equilibrator pressure and was used to obtain the

30   partial pressure of CO_2 in the equilibrator ($pCO_{2(eq)}$).

Ocean Science
Discussions

1   The Licor was calibrated using three CO_2 standard gases before and after each NSOP

2   deployment. The concentrations of the standard gases (BOC Ltd.) were determined by

3   referencing against US National Oceanic and Atmospheric Administration certified standards

4   (244.91, 388.62, 444.40 ppm) in the laboratory. The seawater temperature at the entry and

5   exit ports of the equilibrator was recorded at 1 Hz (Omega ultra-precise 1/10 DIN immersion

6   RTD) using stackable microcontrollers (Tinkerforge master brick 2.1 and PTC bricklet).

7   Equilibrator temperature probes and the miniCTD temperature sensor were calibrated before

8   and after each cruise against an accurate reference sensor (Fluke, model 5616-12, ±0.011°C)

9   in a stable water bath (Fluke 7321).

10
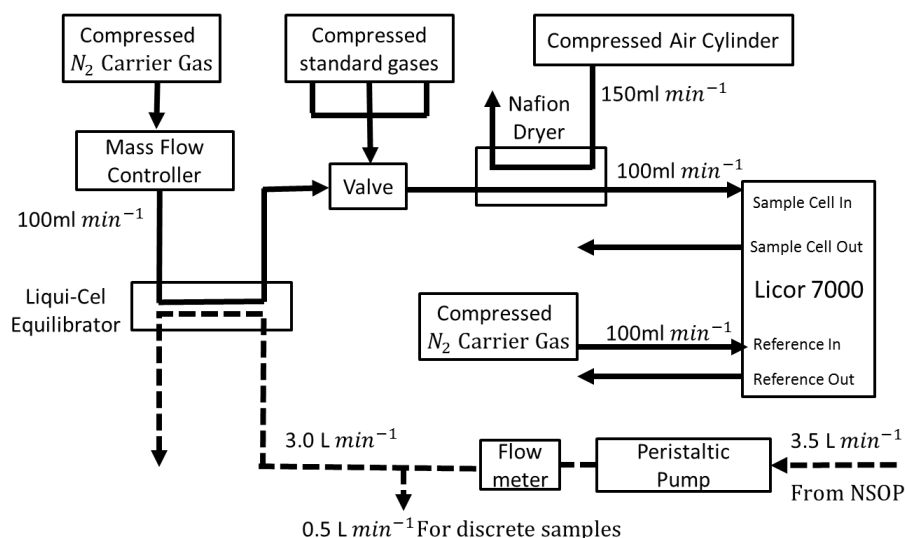
11

12   **Figure 2:** CO_2 system schematic. Solid and dashed arrows correspond to gas and water flows
13   respectively. The Licor reference cell is flushed with equilibrated gas at 100 ml min^{-1}. A
14   manual selection valve was used to switch between equilibrated gas and the CO_2 standards.

15

16   2.3.1   Equilibrator

17   The showerhead equilibrator is the most commonly-used equilibrator for CO_2 but takes ~100

18   s to equilibrate (Dickson et al., 2007; Kitidis et al., 2012; Körtzinger et al., 2000; Webb et al.,

19   2016). This equilibration time is too slow for effective use during NSOP deployments. We

Ocean Science
Discussions
Open Access
EGU

1   used a membrane equilibrator (Liqui-Cel, model 2.5x8) because it has a large surface area to

2   volume ratio and membrane porosity (50%). The Liqui-Cel expedites gas transfer and

3   efficiently achieves equilibration (Loose et al., 2009), with a 3 s response time for CO_2 (Hales

4   et al., 2004). Membrane equilibrators have been used by others for trace gas analysis (Hales et

5   al., 2004; Marandino et al., 2009).

6   Fugacity of seawater CO_2 is calculated from the Licor gas phase CO_2 measurement. This

7   approach assumes that the gas phase sample has equilibrated fully with the seawater. We

8   performed equilibration efficiency experiments in a seawater tank using a showerhead

9   equilibrator as a reference. Liqui-Cel equilibration efficency declined after prolonged

10   exposure to seawater, likely due to biofouling of the membranes. In a fouled equilibrator,

11   equilibration efficency was a function of the flow rate on both the water and gas side of the

12   membrane. An increased gas flow rate reduces the residence time inside the Liqui-Cel and

13   allows less time to equilibrate (Fig. 3a). Increasing the waterside flow rate moves the gas

14   phase closer to equilibrium because the transfer coefficent in the membrane increases (Fig.

15   3b).

16   Cleaning with an acid - base sequence restored the efficiency of a fouled equilibrator. It was

17   necessary to actively pump chemicals through the Liqui-Cel to achieve a full recovery in

18   efficiency. For more details on cleaning techniques, see supplemental material. Efficiency

19   reductions in membrane equilibrators like the Liqui-Cel have not been reported by previous

20   studies. Some authors have used 5-50 µm filters to minimise biofouling (Hales et al., 2004)

21   but this was not possible with the NSOP experimental design. If filtering seawater is not

22   possible, we recommend flushing with freshwater after use, regular cleaning of the Liqui-Cel

23   and daily tests to quantify equilibration efficiency. Trace gas measurement systems that use

24   an internal liquid phase standard (e.g. dimethylsulfide, Section 2.4) account for any changes

25   in equilibrator efficiency.

26

Ocean Science
Discussions

Open Access

EGU
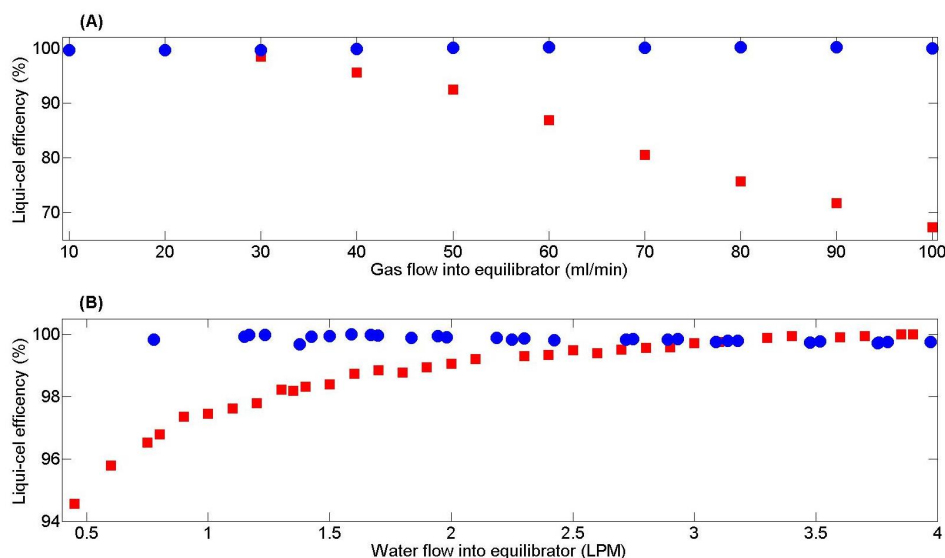
Figure 3: Liqui-Cel CO_2 equilibration efficiency (Liqui-Cel mixing ratio / showerhead mixing ratio) for: (a) changing gas flow at a fixed water flow rate of 4 L min^{-1}; and (b) changing water flow at a fixed gas flow of 100 ml min^{-1}. Blue = unfouled equilibrator. Red = fouled equilibrator.

2.4   DMS analysis

DMS was measured with Atmospheric Pressure-Chemical Ionisation Mass Spectrometry

(API-CIMS), using a system modified following Saltzman et al. (2009). Measurements were

calibrated using an isotopic liquid standard of tri-deuterated DMS (see Bell et al., 2013 for

details). Isotopic standard was injected at 120 μL min^{-1} into the 3 L min^{-1} seawater flow from

NSOP before it entered the Liqui-Cel equilibrator. Compressed nitrogen gas was passed

through the equilibrator in the counter direction to the seawater flow at 1 L min^{-1}. The use of

an internal standard meant that any incomplete equilibration of the ambient non-isotopic DMS

was also true for the isotope. The gas stream exited the equilibrator and was dried (Permapure

nafion dryer, model MD-110-48S-4) before entering the mass spectrometer for analysis. DMS

was detected at m/z 63 and the isotopic standard detected at m/z 66. The concentration of

DMS was calculated using the ion signals and relevant flow rates (Bell et al., 2015). This

approach has been shown to compare well with other analytical techniques for DMS (Walker

et al.., 2016; Royer et al., 2014).

1   **2.5   NSOP response and delay time**

2   The response time of the NSOP setup was determined by simulating step changes in gas

3   concentrations. The tubing inlet was quickly transferred between two buckets of seawater

4   with a distinct difference in concentration. A model fit to the exponential change in signal was

5   used to estimate the response time (Fig. 4). We estimate the system response time (e-folding

6   time) for CO_2 as 24 s, which is slightly faster than the 34 s reported by Webb et al. (2016).

7   The e-folding time in the DMS signal is estimated as 11 s, which is consistent with the rapid

8   gas flow rate through the analytical system.

9   Continuous profiling with the CO_2 system and a 24 s response time yields a depth resolution

10   of 1.2 m, which is greater than the required resolution to assess near surface gradients. DMS

11   has a faster response time than CO_2, but in continuous profiling mode this only translates to a

12   depth resolution of 0.6 m, slightly less than the 1.2-2 m reported by (Royer et al., 2014). A

13   depth resolution of < 0.5 m was desired to capture upper ocean vertical gradients in CO_2 and

14   DMS so NSOP was operated in discrete profiling mode.
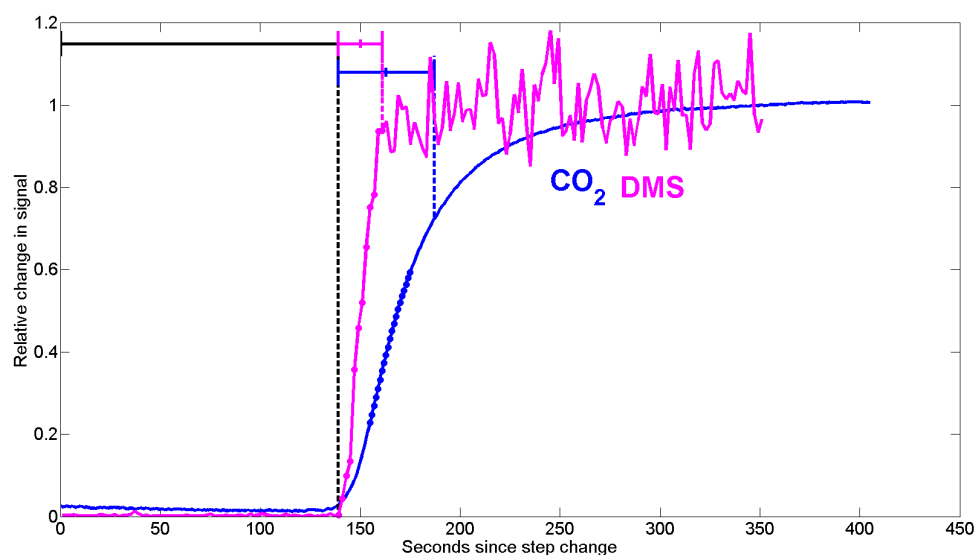
15

16   **Figure 4:** Instrument responses to step changes in seawater CO_2 (blue) and DMS (magenta).
17   Instrument responses have been scaled so that the initial and end concentrations are between 0
18   and 1. Time is referenced against the point when the step change was initiated. The response
19   is seen in both instruments after a delay of 139 s (black dashed line). Two e-foldings are
20   indicated by vertical dashed lines for CO_2 (blue) and DMS (magenta). The data points marked
21   by circles were used to make an exponential fit to the data to determine the response time
22   (Sect 2.5).

1

2   We used different approaches to assess the delay between instantaneous miniCTD

3   measurements and water arriving to the ship for analysis. Using the internal volume of NSOP

4   tubing (0.5 in ID, 54 m length) and a seawater flow rate of 4.15 L min^{-1}, the tubing delay to

5   the equilibrator was calculated as 114 s. Delay correlation analysis between the NSOP

6   miniCTD temperature and a temperature sensor positioned at the entrance to the equilibrator

7   suggests a delay of 112 s. The delay between a bucket switch and a CO_2 change in the Licor

8   was timed at 138 s. The bucket switch delay was longer because the bucket switch experiment

9   also accounts for the delay in the equilibrator and the Licor.

10

11 **2.6   Data processing**

12 During discrete profiling, distinct sample depths were identified from the rapid changes in

13 pressure during depth transitions. Data were binned into discrete depth bins using CTD

14 pressure measurements. Trace gas data were assigned to depth bins after adjusting for the

15 calculated transit time through the NSOP tubing (Section 2.5). CO_2 data from the beginning

16 (2 e-foldings + 15 s buffer = 63 s) and end (15 s buffer) of each depth bin was excluded from

17 analysis to account for the response time of the system and the transition time between sample

18 depths. The same approach was taken for DMS, where the faster response time resulted in a

19 smaller portion of data excluded at the beginning of each depth bin (2 e-foldings + 15 s buffer

20 = 37 s).

21 The CO_2 mixing ratio (xCO_2) measured in the Licor is converted to equilibrator fugacity

22 ($fCO_{2(eq)}$) using calibration standards, *in situ* seawater salinity, and the pressure and

23 temperature in the equilibrator (SOP 5# Underway pCO2Dickson et al., 2007). Vertical

24 profiles of seawater CO_2 fugacity ($fCO_{2(sw)}$) are calculated using average equilibrator fugacity

25 ($fCO_{2(eq)}$), equilibrator temperature ($T_{(eq)}$) and *in situ* seawater temperature ($T_{(sw)}$) at each

26 depth (Takahashi et al., 1993). The time series $fCO_{2(sw)}$ data shown in (Fig. 7) are also

27 calculated using the same equation from Takahashi et al. (1993) but instead use high

28 frequency $fCO_{2(sw)}$, $T_{(eq)}$ and $T_{(sw)}$ data.

Ocean Science
Discussions

EGU

2.7   Seawater sample collection using NSOP

The NSOP setup enables vertical profiles of discrete seawater samples to be collected from upstream of the equilibrator, with a split in the tubing diverting ~0.5 L min^{-1} into a sink. For example, discrete seawater samples (250 ml) have been successfully collected and analysed for Total Alkalinity (TA). Samples were collected and poisoned following best practice recommendations (SOP#1, (Dickson et al., 2007). Bottle filling plus 1 overfill took ~60 s. Start and end times were recorded so that collection depth could be retrospectively determined from the CTD pressure data. Analytical methods and an example depth profile (Fig. S3) are provided in Supplementary information.

3   Field Measurements / Observations

Presented below are example profiles collected using NSOP. The first deployment was in the open ocean (July 30th 2015, Central Celtic Sea; 49.4213°N, -8.5783°E) from the *RRS Discovery* (100 m length, 6.5 m draught). The second deployment was in coastal waters (15th April 2014, Plymouth Sound; 50.348°N, -4.126°E) from the *RV Plymouth Quest* (20 m length, 3 m draught).

3.1   Open ocean deployment

NSOP was deployed at 14:05 (UTC) on 30th July 2015. During the 6 hours preceding deployment, the ship was on station and encountered persistently strong solar radiance (> 600 W m^{-2}), mild winds (< 6 m s^{-1}) and calm sea state (significant wave height < 1.6 m). This combination of low wind speeds and high irradiance (Fig. 5) is favourable for near surface stratification (Donlon et al., 2002).

Ocean Science
Discussions

1
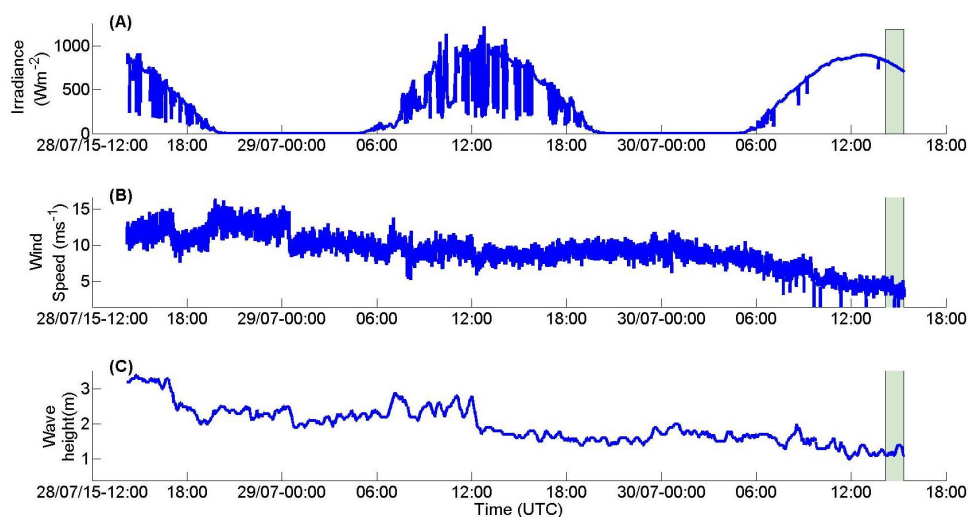
Figure 5: Timeseries of meteorology and sea state variables in the Celtic Cea in July 2015
while the ship was on station: (a) irradiance; (b) wind speed; and (c) significant wave height.
The data begin 48 h before the start of the profile at 14:05 hrs (UTC). The vertical grey bar
indicates the period when NSOP was profiling.

Fig. 6 presents the time series data collected by NSOP for depth, temperature, salinity and

$fCO_{2(sw)}$. Discrete profiling began at 14:05 hrs (UTC) at 0.7 m depth, which was as close to

the surface as the frame could be located without the possibility of breaking the surface.

Depth bins were identified based on rapid depth transitions (Fig. 6a). Bottles were filled for

discrete samples during the downcast. Profiling lasted 75 minutes and finished back at the

surface at 15:20 hrs (UTC). Seawater temperature was 16.61 ± 0.06 °C and $fCO_{2(sw)}$ was

undersaturated with respect to the atmosphere; both were the expected magnitude for summer

in the Celtic Sea (Frankignoulle and Borges, 2001). Salinity was homogeneous throughout the

NSOP deployment, only varying by ±0.004.

Ocean Science
Discussions

1
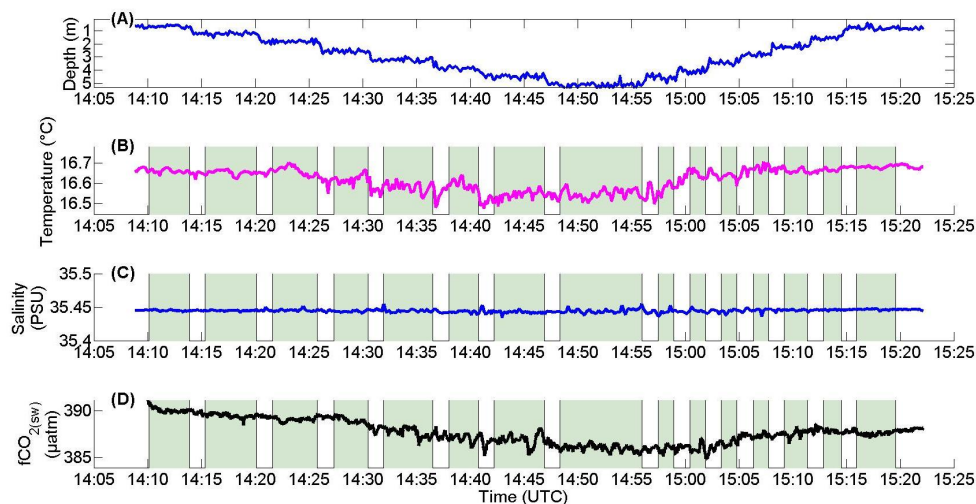
Figure 6: Time series measurements made during an NSOP deployment in the Celtic Sea on
30th July 2015. Data are 1 Hz depth (a), seawater temperature (b), salinity (c) and fCO$_{2(sw)}$ (d).
Data used for depth bin analysis (Section 2.6) is identified by a shaded background.

5

6   Depth-binned salinity and temperature data did not show any significant variability (Fig. 7a).

7   A slight temperature gradient was observed, with 0.15°C difference between 5 m and the

8   surface and a fairly constant reduction with depth (0.03°C per metre). The temperature profile

9   was similar for down and up casts, although some continued warming of surface waters was

10   evident in the up cast. The temperature measured by NSOP at 5.15 m depth agrees well with

11   the coincident temperature measured by the bow thermistor at 5.5 m (< 0.02°C difference)

12   (Fig. 7c). There is no evidence that the ship's thrusters/propellers disrupted the near surface

13   gradients.

14   We compare the NSOP temperature profile with thermistor readings from a series of sensors

15   on a mooring ~2.8 km away (0.3, 0.6, 1.5, 3.5 and 7 m depth). The vertical profile implied by

16   the NSOP deployment agrees with the mooring data (Fig. 7c), and corroborates the warming

17   of the upper few metres of the ocean observed during the deployment. The agreement

18   between these independent datasets suggests that it is unlikely that NSOP caused any

19   significant localized warming of surface waters. The mean difference between NSOP

20   temperature from discrete depths and the mooring sensors is 0.02°C. The surface data from

21   the NSOP up cast show less agreement with the mooring, with NSOP temperatures ~0.05 °C

22   lower than the 0.3 m and 0.6 m mooring sensors. During the profile the ship drifted ~1 km

15

Ocean Science
Discussions

1   from the start position of the profile and a further 0.2 km from the mooring. The small offset

2   between the NSOP surface temperatures and the mooring may be driven by horizontal

3   variability between the deployment and mooring locations. It is also possible that turbulence

4   mixed warm surface waters down into cooler sub-surface layers. Turbulence could have been

5   generated around the NSOP sampling frame or by an increase in wave-driven mixing when

6   the significant wave height increased at ~15:00 hrs UTC (Fig. 5a).
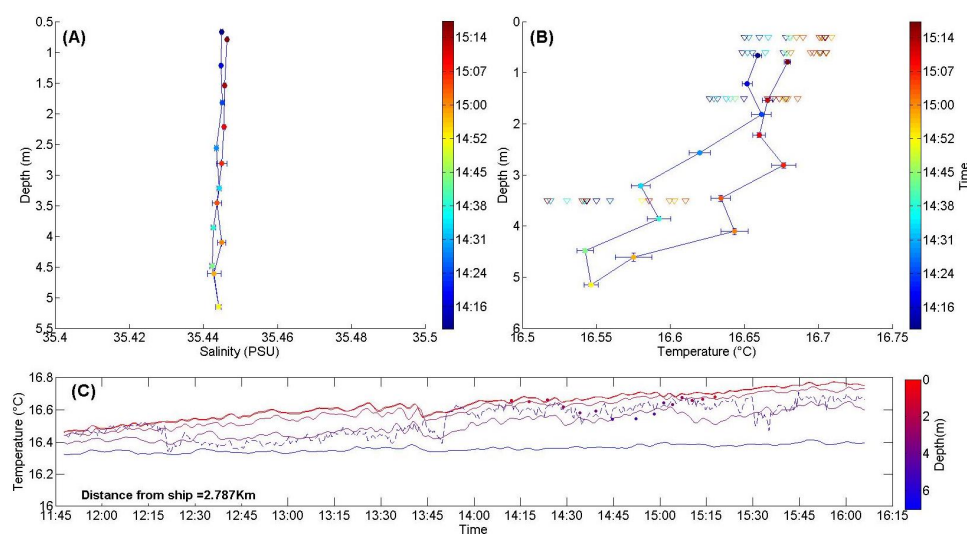
8   **Figure 7:** Salinity and temperature in the Central Celtic Sea on 30th July 2015. NSOP profiles
9   of salinity (a) and temperature (b) were derived using depth bins as described in Section 2.6.
10   Data points are coloured by sampling time. Vertical and horizontal error bars show two
11   standard errors of the mean in each depth bin. Coloured triangles in (B) are time-averaged
12   temperature for four depths (0.3, 0.6, 1.5 and 3.5 m) at the nearby Central Celtic Sea
13   temperature mooring (49.403°N, -8.606°E). (c) Timeseries of temperature at the mooring.
14   Dashed line is the underway temperature at 5.5 m from *RRS Discovery* (located 2.8 km from
15   the mooring). Coloured circles are binned temperature data from NSOP. Sample depth is
16   indicated by blue-red colour, where red is the air/sea interface.

17

18   Seawater density (Fig. 8a) was calculated using the salinity and temperature profile data (Fig.

19   7a &7b) and the 1983 Unesco equation of state (Millero and Poisson, 1981). As expected with

20   little variation in the salinity, changes in the density profile are dominated by temperature.

21   The down and up casts for CO_2 show excellent agreement below 2.5 m. Surface water (< 2 m)

22   CO_2 is 2-4 µatm higher than at 5 m (Fig. 8b). Elevated surface CO_2 could be explained by a

23   sustained flux from the atmosphere into a near surface stratified layer with inhibited deep

Ocean Science
Discussions

1   water exchange. Under this assumption a vertical gradient in seawater CO_2 would need to be

2   established shortly after the temperature gradient. Surface CO_2 is significantly different

3   between the down and up casts. The deepening of the surface stratified layer could explain the

4   more homogeneous CO_2 during the upcast. It is worth noting that in addition to physical

5   processes, plankton trapped within the surface layer could also modify the surface CO_2.
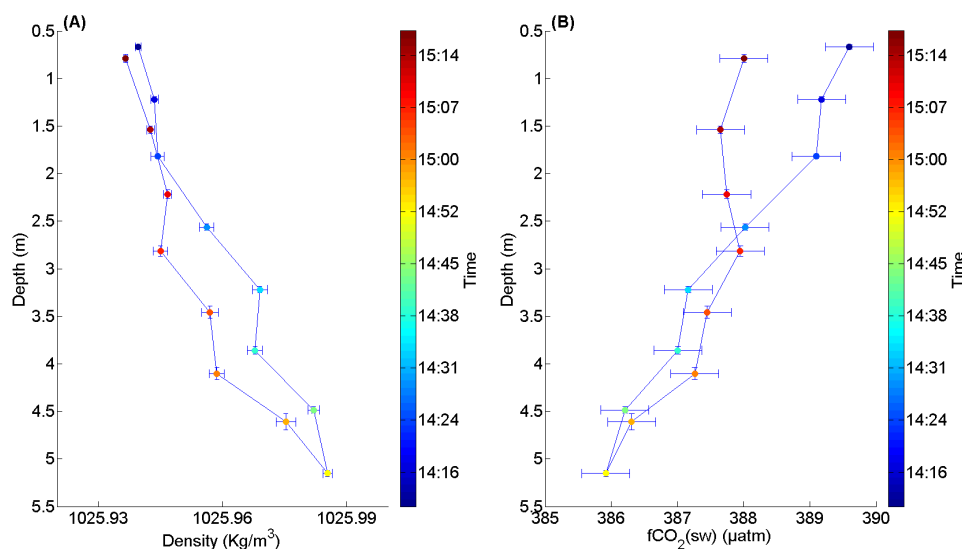
6

7   **Figure 8:** NSOP density (a) and $fCO_{2(sw)}$ (b) profiles from the Celtic Sea on 30th July 2015.
8   Data points are coloured by sample time. Vertical error bars correspond to two standard
9   errors of the mean in each depth bin. The horizontal error bars in (a) are two standard errors of
10   the mean, whereas in (b) they are the propogated error from the the binned measurements used
11   to calculate $fCO_{2(sw)}$.

12

13   To assess measurement accuracy the NSOP Liqui-Cel CO_2 system was compared against an

14   independent CO_2 system that had a showerhead equilibrator coupled to the ship's seawater

15   supply pumped from 5.5 m below the sea surface (Hardman-Mountford et al., 2008; Kitidis et

16   al., 2012). Technical issues meant that the underway CO_2 system installed on the *RRS*

17   *Discovery* was not functioning during the deployment detailed above. However during

18   deployments on the 19th and 20th July, the $fCO_{2(sw)}$ measured by NSOP close to the underway

19   intake depth agrees to within 3 μatm.

20

1 ## 3.2 Coastal deployment

2 DMS profiles were collected on a small research vessel on 15th April 2014. NSOP was

3 deployed within the Plymouth Sound at 12:00 hrs UTC and recovered 95 minutes later (Fig.

4 10). In the sheltered environment behind the breakwater the standard deviation in depth was

5 ±0.10 m, smaller than observed during open ocean profiles. Seawater temperature and salinity

6 demonstrate clear structure, with lower temperatures and higher salinities associated with sub-

7 surface water. Two river estuaries (Plym and Tamar) converge and flow out to the open ocean

8 through the Plymouth Sound. We likely observed a freshwater surface lens that was protected

9 from wave-driven mixing and had been warmed over the course of the day. We used a

10 different miniCTD during this deployment and were thus also able to collect fluorescence

11 data (Fig. 10d).

12 Temperature profiles (Fig. 11a) show a sharp discontinuity in the downcast at ~5 m whereas

13 in the upcast the thermocline had shoaled to ~3.5 m. The salinity profiles suggest similar

14 mixing depths to the temperature profiles, with lower salinity water at the surface (Fig. 10b).

15 Fluorescence increases with depth (Fig. 10c), but this is likely due to quenching of the

16 phytoplankton photosynthetic apparatus at the surface. DMS concentrations reduce steadily

17 with depth (Fig. 10d), which is likely explained by changes in DMS production and

18 consumption rates by the biological community (Galí et al., 2013). The DMS profiles from

19 the upcast and the downcast are very similar, with the largest difference at the very surface. A

20 large difference in the surface-most data point can also be seen in the temperature data, and

21 may reflect mixing with sub-surface waters due to the motion of NSOP or short time-scale

22 variations in the physical environment.

Ocean Science

Discussions

Open Access

1
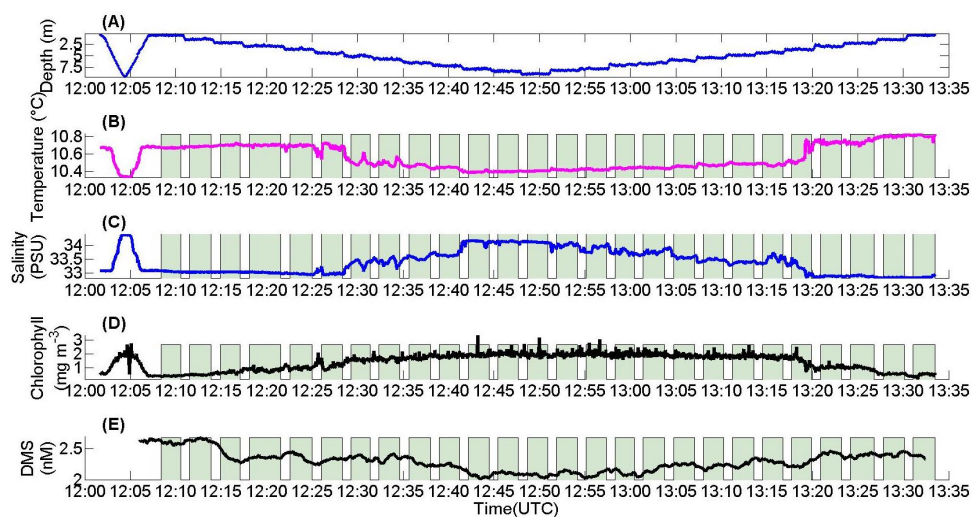
Figure 9: Time series measurements during an NSOP deployment in Plymouth Sound on 15th
April 2014: depth (a), temperature (b), salinity (c), chlorophyll fluorescence (d) and DMS$_{(sw)}$
(e). Data used for depth bin analysis (Section 2.6) is identified by a shaded background.

5
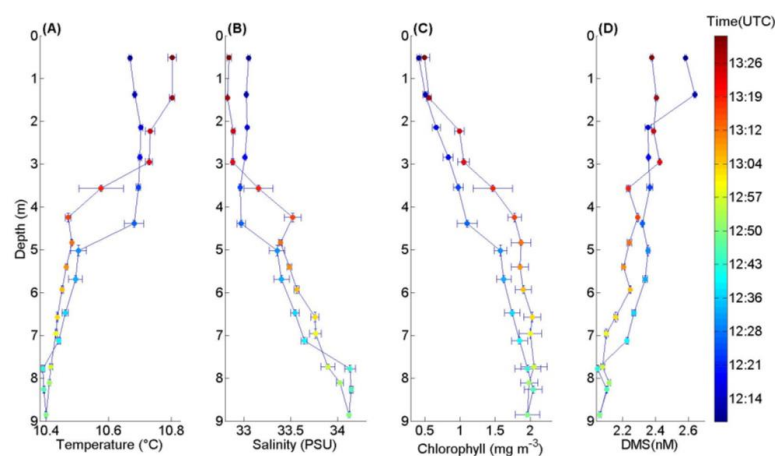
Figure 10: NSOP profiles collected in Plymouth Sound on 15th April 2014: temperature (a),
salinity (b), chlorophyll fluorescence (c), and DMS$_{(sw)}$ (d). Data are coloured by sample time.
Vertical and horizontal error bars are two standard errors of the mean (SEM) in each depth
bin.

11

Ocean Science
Discussions

Open Access

EGU

1 **4   Summary**

2 This paper describes a Near Surface Ocean Profiler (NSOP) designed to measure vertical

3 trace gas profiles near the air-sea interface. NSOP is unique in approach as its sampling frame

4 is lowered from a buoy that rides the ocean swell, reducing relative motion of the frame and

5 hence fluctuations in sampling depth. The NSOP design facilitates near surface (< 0.5 m)

6 sampling, significantly improving the capability to resolve vertical gradients. Other benefits

7 include the ability to sample away from ship-driven turbulence and the flexibility to make a

8 large range of near surface measurements. The NSOP sampling frame houses the miniCTD

9 and also has the capacity to incorporate additional sensors (e.g. dissolved oxygen and other

10 measures of phytoplankton abundance and photosynthetic health). The ability to collect water

11 from discrete depths facilitates the collection of near surface samples that require additional

12 processing or take longer to analyse (e.g. TA, dissolved inorganic carbon, nutrients, the DMS-

13 precursor DMSP, dissolved organic carbon). NSOP is highly versatile and can be used for

14 continuous or discrete profiling. Further development could adjust winch pay out speed and

15 enable continuous, high resolution depth profiles for slower response time measurements (e.g.

16 $fCO_{2(sw)}$).

17 Near surface stratification in the upper few metres of the ocean due to temperature and

18 salinity gradients is a well-documented phenomenon. The presence or absence of chemical

19 and biological gradients within near surface stratified layers has been difficult to assess.

20 NSOP is a platform with the capability to successfully resolve gradients in these near surface

21 layers.

22

Ocean Science
Discussions

1

References

Bakker, D. C. E., Pfeil, B., Landa, C. S., Metzl, N., O'Brien, K. M., Olsen, A., Smith, K., Cosca, C., Harasawa, S., Jones, S. D., Nakaoka, S. I., Nojiri, Y., Schuster, U., Steinhoff, T., Sweeney, C., Takahashi, T., Tilbrook, B., Wada, C., Wanninkhof, R., Alin, S. R., Balestrini, C. F., Barbero, L., Bates, N. R., Bianchi, A. A., Bonou, F., Boutin, J., Bozec, Y., Burger, E. F., Cai, W. J., Castle, R. D., Chen, L., Chierici, M., Currie, K., Evans, W., Featherstone, C., Feely, R. A., Fransson, A., Goyet, C., Greenwood, N., Gregor, L., Hankin, S., Hardman-Mountford, N. J., Harlay, J., Hauck, J., Hoppema, M., Humphreys, M. P., Hunt, C. W., Huss, B., Ibánhez, J. S. P., Johannessen, T., Keeling, R., Kitidis, V., Körtzinger, A., Kozyr, A., Krasakopoulou, E., Kuwata, A., Landschützer, P., Lauvset, S. K., Lefèvre, N., Lo Monaco, C., Manke, A., Mathis, J. T., Merlivat, L., Millero, F. J., Monteiro, P. M. S., Munro, D. R., Murata, A., Newberger, T., Omar, A. M., Ono, T., Paterson, K., Pearce, D., Pierrot, D., Robbins, L. L., Saito, S., Salisbury, J., Schlitzer, R., Schneider, B., Schweitzer, R., Sieger, R., Skjelvan, I., Sullivan, K. F., Sutherland, S. C., Sutton, A. J., Tadokoro, K., Telszewski, M., Tuma, M., Van Heuven, S. M. A. C., Vandemark, D., Ward, B., Watson, A. J., and Xu, S.: A multi-decade record of high-quality fCO_2 data in version 3 of the Surface Ocean CO_2 Atlas (SOCAT), Earth Syst. Sci. Data Discuss., 2016, 1-55, 10.5194/essd-2016-15, 2016.

Bange, H. W., Bell, T. G., Cornejo, M., Freing, A., Uher, G., Upstill-Goddard, R. C., and Zhang, G.: MEMENTO: a proposal to develop a database of marine nitrous oxide and methane measurements, Environmental Chemistry, 6, 195-197, 2009.

Bell, T., De Bruyn, W., Miller, S., Ward, B., Christensen, K., and Saltzman, E.: Air–sea dimethylsulfide (DMS) gas transfer in the North Atlantic: evidence for limited interfacial gas exchange at high wind speed, Atmospheric Chemistry and Physics, 13, 11073-11087, 2013.

Bell, T., De Bruyn, W., Marandino, C. A., Miller, S., Law, C., Smith, M., and Saltzman, E.: Dimethylsulfide gas transfer coefficients from algal blooms in the Southern Ocean, Atmospheric Chemistry and Physics, 15, 1783-1794, 2015.

Dickson, A. G., Sabine, C. L., and Christian, J. R.: Guide to best practices for ocean CO_2 measurements, 2007.

Donlon, C., Minnett, P., Gentemann, C., Nightingale, T., Barton, I., Ward, B., and Murray, M.: Toward improved validation of satellite sea surface skin temperature measurements for climate research, Journal of Climate, 15, 353-369, 2002.

Durham, W. M., Kessler, J. O., and Stocker, R.: Disruption of vertical motility by shear triggers formation of thin phytoplankton layers, Science, 323, 1067-1070, 2009.

Fairall, C., Bradley, E. F., Godfrey, J., Wick, G., Edson, J. B., and Young, G.: Cool-skin and warm-layer effects on sea surface temperature, Journal of Geophysical Research, 101, 1295-1308, 1996.

Frankignoulle, M., and Borges, A. V.: European continental shelf as a significant sink for atmospheric carbon dioxide, Global Biogeochemical Cycles, 15, 569-576, 2001.

Galí, M., Simó, R., Vila-Costa, M., Ruiz-González, C., Gasol, J. M., and Matrai, P.: Diel patterns of oceanic dimethylsulfide (DMS) cycling: Microbial and physical drivers, Global Biogeochemical Cycles, 27, 620-636, 2013.

Ocean Science
Discussions

1   Hales, B., Chipman, D., and Takahashi, T.: High-frequency measurement of partial pressure
2   and total concentration of carbon dioxide in seawater using microporous hydrophobic
3   membrane contractors, Limnol. Oceanogr.: Methods 2, 356-364, 2004.

4   Hardman-Mountford, N. J., Moore, G., Bakker, D. C., Watson, A. J., Schuster, U., Barciela,
5   R., Hines, A., Moncoiffé, G., Brown, J., and Dye, S.: An operational monitoring system to
6   provide indicators of CO_2-related variables in the ocean, ICES Journal of Marine Science:
7   Journal du Conseil, 65, 1498-1503, 2008.

8   Kitidis, V., Hardman-Mountford, N. J., Litt, E., Brown, I., Cummings, D., Hartman, S.,
9   Hydes, D., Fishwick, J. R., Harris, C., and Martinez-Vicente, V.: Seasonal dynamics of the
10 carbonate system in the Western English Channel, Continental Shelf Research, 42, 30-40,
11 2012.

12 Körtzinger, A., Mintrop, L., Wallace, D. W., Johnson, K. M., Neill, C., Tilbrook, B., Towler,
13 P., Inoue, H. Y., Ishii, M., and Shaffer, G.: The international at-sea intercomparison of fCO_2
14 systems during the R/V Meteor Cruise 36/1 in the North Atlantic Ocean, Marine Chemistry,
15 72, 171-192, 2000.

16 Lana, A., Bell, T., Simó, R., Vallina, S. M., Ballabrera-Poy, J., Kettle, A., Dachs, J., Bopp, L.,
17 Saltzman, E., and Stefels, J.: An updated climatology of surface dimethlysulfide
18 concentrations and emission fluxes in the global ocean, Global Biogeochemical Cycles, 25,
19 2011.

20 Le Quéré, C., Andrew, R. M., Canadell, J. G., Sitch, S., Korsbakken, J. I., Peters, G. P.,
21 Manning, A. C., Boden, T. A., Tans, P. P., and Houghton, R. A.: Global carbon budget 2016,
22 Earth System Science Data, 8, 605, 2016.

23 Liss, P. S., and Slater, P. G.: Flux of Gases across the Air-Sea Interface, Nature, 247, 181-
24 184, 1974.

25 Loose, B., Stute, M., Alexander, P., and Smethie, W.: Design and deployment of a portable
26 membrane equilibrator for sampling aqueous dissolved gases, Water Resources Research, 45,
27 2009.

28 Marandino, C. A., De Bruyn, W. J., Miller, S. D., and Saltzman, E. S.: Open ocean DMS
29 air/sea fluxes over the eastern South Pacific Ocean, Atmos. Chem. Phys., 9, 345-356,
30 10.5194/acp-9-345-2009, 2009.

31 McNeil, C. L., and Merlivat, L.: The warm oceanic surface layer: Implications for CO_2 fluxes
32 and surface gas measurements, Geophysical research letters, 23, 3575-3578, 1996.

33 Miller, S. D., Marandino, C., and Saltzman, E. S.: Ship-based measurement of air-sea CO_2
34 exchange by eddy covariance, Journal of Geophysical Research: Atmospheres, 115, 2010.

35 Millero, F. J., and Poisson, A.: International one-atmosphere equation of state of seawater,
36 Deep Sea Research Part A. Oceanographic Research Papers, 28, 625-629, 1981.

37 Quinn, P., and Bates, T.: The case against climate regulation via oceanic phytoplankton
38 sulphur emissions, Nature, 480, 51-56, 2011.

39 Robertson, J. E., and Watson, A. J.: Thermal skin effect of the surface ocean and its
40 implications for CO_2 uptake, Nature, 358, 738-740, 1992.

41 Royer, S.-J., Galí, M., Saltzman, E. S., McCormick, C. A., Bell, T. G., and Simó, R.:
42 Development and validation of a shipboard system for measuring high-resolution vertical

Ocean Science
Discussions

1 profiles of aqueous dimethylsulfide concentrations using chemical ionisation mass
2 spectrometry, Environmental Chemistry, 11, 309-317, 2014.

3 Royer, S. J., Galí, M., Mahajan, A. S., Ross, O. N., Pérez, G. L., Saltzman, E. S., and Simó,
4 R.: A high-resolution time-depth view of dimethylsulphide cycling in the surface sea,
5 Scientific Reports, 6, 32325, 2016.

6 Saltzman, E. S., De Bruyn, W. J., Lawler, M., Marandino, C., and McCormick, C.: A
7 chemical ionization mass spectrometer for continuous underway shipboard analysis of
8 dimethylsulfide in near-surface seawater, Ocean Science, 5, 537-546, 2009.

9 Smyth, T. J., Fishwick, J. R., Lisa, A.-M., Cummings, D. G., Harris, C., Kitidis, V., Rees, A.,
10 Martinez-Vicente, V., and Woodward, E. M.: A broad spatio-temporal view of the Western
11 English Channel observatory, Journal of Plankton Research, 32, 585-601, 2010.

12 Takahashi, T., Olafsson, J., Goddard, J. G., Chipman, D. W., and Sutherland, S.: Seasonal
13 variation of CO_2 and nutrients in the high-latitude surface oceans: A comparative study,
14 Global Biogeochemical Cycles, 7, 843-878, 1993.

15 Turk, D., Zappa, C. J., Meinen, C. S., Christian, J. R., Ho, D. T., Dickson, A. G., and
16 McGillis, W. R.: Rain impacts on CO_2 exchange in the western equatorial Pacific Ocean,
17 Geophysical Research Letters, 37, 2010.

18 Wanninkhof, R.: Relationship between wind speed and gas exchange over the ocean revisited,
19 Limnol. Oceanogr. Methods, 12, 351-362, 2014.

20 Ward, B., Wanninkhof, R., McGillis, W. R., Jessup, A. T., DeGrandpre, M. D., Hare, J. E.,
21 and Edson, J. B.: Biases in the air-sea flux of CO_2 resulting from ocean surface temperature
22 gradients, Journal of Geophysical Research: Oceans (1978–2012), 109, 2004.

23 Webb, J. R., Maher, D. T., and Santos, I. R.: Automated, in situ measurements of dissolved
24 CO_2, CH_4, and δ13C values using cavity enhanced laser absorption spectrometry: Comparing
25 response times of air-water equilibrators, Limnology and Oceanography: Methods, 14, 323-
26 337, 2016.

27 Woolf, D., Land, P. E., Shutler, J. D., Goddijn-Murphy, L., and Donlon, C. J.: On the
28 calculation of air-sea fluxes of CO_2 in the presence of temperature and salinity gradients,
29 Journal of Geophysical Research: Oceans, 2016.

30 Yang, M., Beale, R., Smyth, T., and Blomquist, B.: Measurements of OVOC fluxes by eddy
31 covariance using a proton-transfer-reaction mass spectrometer–method development at a
32 coastal site, Atmospheric Chemistry and Physics, 13, 6165-6184, 2013.

33 Ziska, F., Quack, B., Abrahamsson, K., Archer, S., Atlas, E., Bell, T., Butler, J., Carpenter,
34 L., Jones, C., and Harris, N.: Global sea-to-air flux climatology for bromoform,
35 dibromomethane and methyl iodide, Atmospheric Chemistry and Physics, 13, 8915-8934,
36 2013.

37

38